Shell structure in faceted metal clusters

Nicolas Pavloff
Division de Physique Théorique, Institut de Physique Nucléaire, F-91406 Orsay Cedex, France

Stephen C. Creagh
Niels Bohr Institute, Blegdamsvej 17, DK-2100 Copenhagen Ø, Denmark
(Received 14 June 1993)

We study the quantized electronic energy levels in a three-dimensional icosahedral billiard modeling a faceted metal cluster. The first 2000 levels are determined numerically. The magic numbers are compared with experimental data and with the results for a spherical model. We discuss the supershell structure and propose its study as a test of cluster sphericity. We compare our results with the predictions of the semiclassical trace formula and point out the relevance of diffractive orbits.

I. INTRODUCTION

Recent experiments on molecular beams have allowed investigation of the stability of large metal clusters[1,2] containing up to 20 000 atoms.[3] The most stable clusters—corresponding to "magic" numbers of electrons—fall roughly into one of the following two types: (1) For relatively large numbers of electrons and low temperature they seem to have icosahedral symmetry corresponding to dense packing of the ionic background.[3,4] These are called atomic magic numbers. (2) For higher temperature and/or a lower number of electrons there are electronic magic numbers corresponding to closing of major quantal shells.[1,2,5]

The electronic shell structure in spherical clusters corresponding to case (2) has been studied both theoretically[6,7] and experimentally,[8,9] and has been found to be deeply connected with classical electronic motion. We wish to compare quantum and classical pictures in faceted clusters in the same way. Existing studies of quantum electronic behavior in large and faceted metal clusters[10,11] all consider in some manner that the faceted structure is a perturbation of a spherical arrangement. However, such an approach would not be appropriate for our purposes because it would obscure any link with a classical study, where—as we will see—the faceting can by no means be considered to be a perturbation.

We have therefore chosen a simple model allowing for a detailed investigation of both classical and quantal problems. N electrons are considered to be moving independently in an infinite potential well having a perfect icosahedral shape with volume V (we speak below of an "icosahedral billiard"). The size of the box is scaled so that the mean electronic density N/V is kept constant and equal to its bulk value. This kind of model can be justified by the "jellium plus mean field" approximation, which is believed to be adequate for alkali metals and to a lesser extent for noble metals. For nonfaceted clusters of these elements, both spherical potential wells and less schematic electronic mean-field models lead to similar patterns for the shell structure (see, e.g., Refs. 6, 12, and 13). Similarly, we believe that the use of a more realistic potential for a faceted cluster would not alter the physical picture presented here.

We choose the icosahedron because this shape has been clearly identified in molecular beams[3,4] and also via electron microscopy in the physics of ultrafine particles.[14] The internal structure of these aggregates could be multiply twined [i.e., formed by a juxtaposition of several crystalline pieces (for a recent review see, e.g., Ref. 15)] or formed by onionlike addition of geometrical shells of atoms to a rigid core,[4] or even disordered, but in accordance with our free-electron model this will be of no relevance for shell structure. Of greater importance would be the bumps on the surface caused by the granularity of the ionic background. However, the effects of random irregularities should compensate when considering an ensemble of clusters—in a beam for instance—whereas faceting is a systematic property. This point is discussed in detail in Appendix A. Moreover, we argue in Appendix B that typical energies linked to faceting are larger by a factor of order $N^{1/3}$ than these caused by small defects of the surface.

In the present paper we expose those aspects of our study that are relevant to the physics of metal clusters. A more detailed account of the solution of the classical problem, including a discussion of the use of semiclassical trace formulas, will be given elsewhere.[16] The present paper is divided as follows. In Sec. II we present the method we use to solve the quantum-mechanical problem. Readers mostly interested in a discussion of shell effects can skip this part and go directly to Sec. III, where we present our results. In Sec. IV we sketch the semiclassical analysis and stress the importance of diffractive effects in the icosahedron. Finally we compare to experimental data and present our conclusions in Sec. V.

II. SOLUTION OF THE QUANTUM PROBLEM

For our model, the quantum-mechanical problem reduces to the Helmholtz equation with Dirichlet boundary conditions on the surface of the icosahedron. To solve this problem, we make the following ansatz for the wave function as a sum over free particle solutions in spherical

polar coordinates:

$$\Psi^{\alpha}(r,\hat{\mathbf{e}})=\sum_{i=1}^{i_{\max}} c_i j_l(kr) S^{\alpha}_{i,n=1}(\hat{\mathbf{e}}) \ . \tag{1}$$

Here the angular functions $S^{\alpha}_{i,n}$ are linear combinations of spherical harmonics, chosen to transform according to a given symmetry class α and described in more detail below. The $j_l(kr)$ are the spherical Bessel functions, l being the angular momentum associated with the labels (α,i).

For a given k, the summation in (1) extends up to $i_{\max}$, which is chosen so that the corresponding $j_{l_{\max}}(kr)$ is negligibly small over the whole volume of the icosahedron. More precisely, if $R_{\max}$ is the largest distance from the surface to the center of the icosahedron, $l_{\max}$ is defined by

$$l_{\max} \simeq [kR_{\max}] \ , \tag{2}$$

where the square brackets denote the integer part. The stability of the final results with respect to changes of $i_{\max}$ will provide a good test of the numerical accuracy.

The wave vector k and the c_i's are determined by imposing the boundary conditions. If the surface of the icosahedron is defined by $r=r_B(\hat{\mathbf{e}})$, these conditions read explicitly

$$\Psi^{\alpha}(r_B(\hat{\mathbf{e}}),\hat{\mathbf{e}})=0 \ , \tag{3}$$

for all unit vectors $\hat{\mathbf{e}}$.

Before describing the method of solution of (3), let us briefly discuss the symmetry group I_h, and define the symmetry-adapted angular functions $S^{\alpha}_{i,n}$. I_h is a finite subgroup of $O(3)$, consisting of 60 proper rotations and 60 rotations with inversion, giving 120 elements in all. It has ten nonequivalent irreducible representations (irreps), which we label by α, and which have dimension $d^{\alpha}=1$, 3, 4, or 5. Let us fix a concrete realization of each irrep α through the set of 120 $d^{\alpha}\times d^{\alpha}$ unitary matrices $U_{\alpha}(g)$, where g denotes an element of I_h. Then, corresponding to this set of U^{α}'s, one can construct the linear combinations of spherical harmonics $S^{\alpha}_{i,n}(\hat{\mathbf{e}})$ which transform under the action of an element g of I_h as follows:

$$gS^{\alpha}_{i,n}(\hat{\mathbf{e}})=S^{\alpha}_{i,n}(g^{-1}\hat{\mathbf{e}})=\sum_{m=1}^{d^{\alpha}} U^{\alpha}_{mn}(g) S^{\alpha}_{i,m}(\hat{\mathbf{e}}) \ . \tag{4}$$

The index i labels the distinct symmetry-adapted functions and runs from 1 to ∞. Each value of i corresponds to a fixed angular momentum l. The index n corresponds to a basis label in the choice of basis for the matrices $U^{\alpha}(g)$, and runs from 1 to d^{α}.

Note that the most general wave function would be expressed as a sum of d^{α} functions of type (1) with $n=1,\ldots,d^{\alpha}$. However, the index n is not an essential quantum number: solutions with the same (α,i) and different n are degenerate and do not mix under an application of the Hamiltonian. Thus we can arbitrarily fix $n=1$, as we do in Eq. (1). This amounts to demanding that the eigenfunction transforms according to the first basis vector of the explicit irrep U^{α}.

To impose boundary condition (3), we use an improved version of the "point matching" method of Schmit.[17] On the boundary, Ψ^{α} can be written as

$$\Psi^{\alpha}(r_B(\hat{\mathbf{e}}),\hat{\mathbf{e}})=\sum_{j=1}^{i_{\max}}\sum_{m=1}^{d^{\alpha}} \gamma_{j,m} S^{\alpha}_{j,m}(\hat{\mathbf{e}}) \ . \tag{5}$$

According to the discussion above, we are free to restrict this sum to $m=1$. The γ's can be treated like Fourier coefficients. We can project a given coefficient $\gamma_{j,m}$ by integrating Eq. (5) against the corresponding symmetry-adapted function as follows:

$$\gamma_{j,m=1}=\int d\Omega\, S^{\alpha *}_{j,1}(\hat{\mathbf{e}})\Psi(r_B(\hat{\mathbf{e}}),\hat{\mathbf{e}})=\sum_{i=1}^{i_{\max}} c_i M^{\alpha}_{ij}(k) \ , \tag{6}$$

where the star denotes complex conjugation and

$$M^{\alpha}_{ij}(k)=\int d\Omega\, j_l(kr_B(\hat{\mathbf{e}})) S^{\alpha *}_{j,1}(\hat{\mathbf{e}}) S^{\alpha}_{i,1}(\hat{\mathbf{e}}) \ . \tag{7}$$

Imposing that Ψ^{α} be zero on the boundary is equivalent to forcing all the γ's to zero. This, in turn, is equivalent to imposing that the determination of the matrix $M^{\alpha}(k)$ be zero:

$$\det\{M^{\alpha}_{ij}(k)\}=0 \ , \quad 1\le i,j\le i_{\max} \ . \tag{8}$$

The solution of this equation gives the eigenlevels belonging to the irrep α.

We can use the symmetry of the boundary to restrict the integration in Eq. (7) to a single face as follows, greatly simplifying the practical implementation of the process. We divide the icosahedron into 120 elementary cells $\mathcal{C}_1\ldots\mathcal{C}_{120}$. A given cell $\mathcal{C}_g$ is mapped onto $\mathcal{C}_1$ by a unique element g of the group: $g\mathcal{C}_g=\mathcal{C}_1$. In cell $\mathcal{C}_g$ we make the change of variable $\hat{\mathbf{e}}\to g\hat{\mathbf{e}}$ and Eq. (7) then reads

$$M^{\alpha}_{ij}(k)=\sum_{g\in I_h}\int_{\mathcal{C}_1} d\Omega\, j_l(kr_B(\hat{\mathbf{e}})) S^{\alpha *}_{j,1}(g\hat{\mathbf{e}}) S^{\alpha}_{i,1}(g\hat{\mathbf{e}}) \ . \tag{9}$$

Using Eq. (4) and the orthonormality of irreducible representation matrices (see e.g., Ref. 18, Chap. 3.5), we have

$$\sum_{g\in I_h} S^{\alpha *}_{j,m}(g\hat{\mathbf{e}}) S^{\alpha}_{i,l}(g\hat{\mathbf{e}})=\frac{120}{d^{\alpha}}\delta_{m,l}\sum_{n=1}^{d^{\alpha}} S^{\alpha *}_{j,n}(\hat{\mathbf{e}}) S^{\alpha}_{i,n}(\hat{\mathbf{e}}) \ , \tag{10}$$

and so the final form of the matrix element is

$$M^{\alpha}_{ij}(k)=\frac{120}{d^{\alpha}}\int_{\mathcal{C}_1} d\Omega\, j_l(kr_B(\hat{\mathbf{e}}))\sum_{n=1}^{d^{\alpha}} S^{\alpha *}_{j,n}(\hat{\mathbf{e}}) S^{\alpha}_{i,n}(\hat{\mathbf{e}}) \ . \tag{11}$$

This form is very useful if one expresses the icosahedral harmonics as linear combinations of spherical harmonics with the z axis going through the center F_1 of the face of cell $\mathcal{C}_1$. Then $r_B(\hat{\mathbf{e}})=OF_1/\cos\theta$ (θ being the azimuthal angle, and O the origin), and the integration over φ in (11) is straightforward. The remaining integration over θ in (11) is done numerically. We have checked that a 34-point Gaussian integration formula[19] provides excellent accuracy up to the highest value of k considered.

The eigenvalues were found by this numerical integration of Eq. (11), followed by a root search for the zeros of $\det\{M^{\alpha}(k)\}$.

III. ANALYSIS OF THE RESULTS

The solution of the quantum-mechanical problem in an icosahedron with edge length a yields a series of eigenlevels $\{k_n\}_{n\geq 0}$ which scale trivially with a. We have computed these levels numerically up to $k_n a \approx 40$. The levels have a group-theoretical degeneracy d_n, where d_n can take values of 1, 3, 4, or 5 (if the associated wave function belongs to irrep α, then $d_n = d^\alpha$, see Sec. II), and a spin degeneracy $\nu = 2$. For a cluster containing N electrons, the edge length a is fixed by the relation $N/V = (4/3\pi r_s^3)^{-1}$, r_s being the Wigner-Seitz radius of the bulk material. "Spill-out" effects can be taken into account phenomenologically by increasing the value of r_s used to determine the dimensions of the box. For instance, in Ref. 6 a value of 2.25 Å was taken for sodium instead of the bulk value $r_s = 2.08$ Å. The level density is

$$\rho(k) = \nu \sum_n d_n \delta(k - k_n) , \tag{12}$$

and the integrated level density (or spectral staircase function) is

$$N(k) = \nu \sum_n d_n \theta(k - k_n) . \tag{13}$$

The functions $N(k)$ and $\rho(k)$ can be separated into the sum of smooth parts $\bar{N}(k)$ and $\bar{\rho}(k)$ and oscillating parts $\tilde{N}(k)$ and $\tilde{\rho}(k)$, respectively. In our three-dimensional case $\bar{N}(k)$ increases roughly like k^3 with some surface and edge corrections. The formula reads (see, e.g., Ref. 20, Chap. VI.2)

$$\bar{N}(k) = a_v (ak)^3 - a_s (ak)^2 + a_l (ak) + \dots , \tag{14}$$

where a_v, a_s, and a_l are dimensionless coefficients which are related to the volume V, surface area S, and angle α between two adjacent faces, according to the formulas

$$a_v = \frac{\nu}{6\pi^2}\left[\frac{V}{a^3}\right] , \quad a_s = \frac{\nu}{16\pi}\left[\frac{S}{a^2}\right] , \quad a_l = \frac{5\nu}{4\pi}\left[\frac{\pi}{\alpha} - \frac{\alpha}{\pi}\right] . \tag{15}$$

We compared the numerically computed smooth part $\bar{N}(k)$ of the spectral staircase function with the expansion in Eq. (14), and found that the agreement was very good. Equation (14) was correct to an overall accuracy of 0.05%—this places typical limits of 0.05%, 0.2%, and 5% on the errors of a_v, a_s, and a_l, respectively, over the range of k examined, so that the numerical spectrum is in detailed agreement with the geometry of the icosahedron. This also indicates that we do not miss any levels in the icosahedron's spectrum. We performed other checks of our numerical procedure: we changed the value of $i_{\max}$ in (1) [going up to $[kR_{\max}]+7$ in formula (2)]; we changed the number of points of integration in (11); and we took both complex and real icosahedral harmonics in (1). All these checks indicate that the eigenlevels are determined with an accuracy of the order of a few hundredths of a level spacing.

From $\bar{\rho}(k)$ or other smoothed quantities one can determine thermodynamical quantities such as the bulk Fermi energy, but the finite-size effects linked to the discreteness of the spectrum manifest themselves in oscillating quantities such as $\tilde{\rho}(k)$. For instance, a minimum in $\tilde{\rho}(k)$ indicates a region of the spectrum with relatively fewer levels, and consequently implies a gap in the ionization potential. Typical experiments study the relative abundance of clusters on a mass spectrum, and these measurements are obviously affected by the degree of ionization of the clusters before arriving in the spectrometer. Accordingly the relevant observables are the total energy, which determines the probability of formation of differently sized clusters in the first place, and the ionization potential, which determines the probability and degree of ionization.

Our model does not have a well-defined ionization potential—since it is an infinite potential well—but essentially the same qualitative information is provided by the Fermi energy E_f. This is defined for a cluster of size N by

$$E_f(N) = \frac{\hbar^2 k_f^2}{2m} \quad \text{where } N(k_f) = N . \tag{16}$$

It can be written as the sum of a smooth N-dependent quantity $\bar{E}_f$ and an oscillating part $\tilde{E}_f$. These oscillations around the smooth curve indicate the presence of shell effects. However, on the basis of semiclassical arguments (see Appendix C) one can show that $\tilde{E}_f$ decreases like $N^{-2/3}$ relative to $\bar{E}_f$, so the shell effects are not easily studied with this observable.

On the other hand, the total energy $E_{\rm tot}$ and its oscillating part $\tilde{E}_{\rm tot}$ do not exhibit such a rapid decrease with N and are therefore more useful for understanding shell effects. The energy $E_{\rm tot}$ is defined by

$$E_{\rm tot}(N) = \int_0^{k_f} \frac{\hbar^2 k^2}{2m} \rho(k) dk = \nu \sum_n{}' d_n \frac{\hbar^2 k_n^2}{2m} , \tag{17}$$

where the prime indicates that the summation extends only over occupied orbitals. Its smooth approximation $\bar{E}_{\rm tot}$ is defined as

$$\bar{E}_{\rm tot}(N) = \int_0^{\bar{k}_f} \frac{\hbar^2 k^2}{2m} \bar{\rho}(k) dk . \tag{18}$$

From Eqs. (14), (16), and (18), we obtain

$$\bar{E}_{\rm tot}(N) = \varepsilon_f \left[\frac{3a_v}{5}\left[\frac{N}{a_v}\right] + \frac{a_s}{2}\left[\frac{N}{a_v}\right]^{2/3} + \frac{a_s^2 - 2a_l a_v}{3a_v}\left[\frac{N}{a_v}\right]^{1/3} + \cdots \right] , \tag{19}$$

where ε_f is the bulk Fermi energy:

$$\varepsilon_f = \frac{\hbar^2}{2mr_s^2}\left[\frac{9\pi}{2\nu}\right]^{2/3} . \tag{20}$$

In Fig. 1 we plot the oscillating part $\tilde{E}_{\rm tot} = E_{\rm tot} - \bar{E}_{\rm tot}$. The presence of magic numbers is clearly seen in this figure. Using the results of Ref. 24 we will point out in

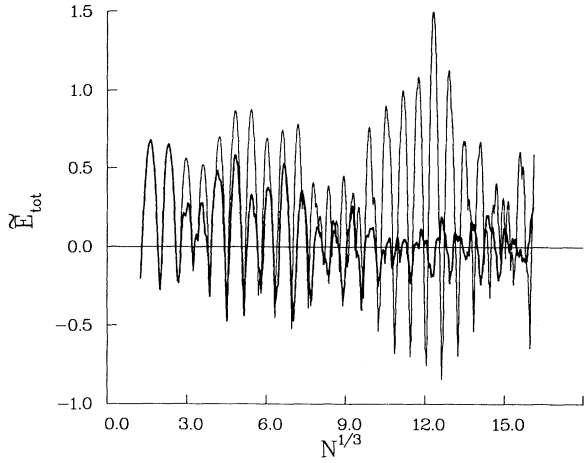

FIG. 1. Oscillating part of the total energy as a function of $N^{1/3}$. $\tilde{E}_{tot}$ is expressed in units of ε_f. The thick line represents the results in the icosahedron, the thin line is for the sphere.

Sec. IV that the bunching of levels leading to shell structure here does not come from degeneracies due to the discrete icosahedral symmetry, but from a local continuous symmetry corresponding to the translation of classical orbits parallel to the faces of the icosahedron. While in the case of the sphere (or any spherically symmetric system) the shell effect in $\tilde{E}_{tot}$ increases like $N^{1/6}$ (see, e.g., Ref. 21), $\tilde{E}_{tot}$ is expected to be approximately constant for large N. We give a semiclassical interpretation of this behavior in Appendix C.

For comparison we also show in Fig. 1 the oscillating part of the total energy for a spherical infinite potential well. The two curves are very similar up to $N \simeq 350$ ($N^{1/3} \simeq 7$). For instance, the magic numbers of the two systems are almost equal up to this value (see Table I).

TABLE I. Magic numbers for the sphere and icosahedron compared with experimental results. The columns Na Stuttgart, Na KBH, and Li Orsay refer to the results of Refs. 3, 8, and 2, respectively.

Sphere	Icosahedron	Na Stuttgart	Na KBH	Li Orsay
2	2	2		2
8	8	8		8
20	20	20		20
34	34	40	40	40
58	58	58	58	58/70
92	92	92	92	92
138	138	138	138	138
186	196	198±2	198	198
254	254	263±5	264	258
338	348	341±5	344	336
440	456	443±5	442	440
542/556	588	557±5	554	546
612/676	708	700±15	680	710
748/832	888	840±15	800	750/820
912			970	910
1074	1076	1040±20	1120	1065/1160
1284	1250	1220±20	1310	1270/1370

This behavior might be expected since electrons can only discriminate between an icosahedron and a sphere when the difference between the radii of the two systems ($\Delta R \simeq 0.1a$) is an appreciable fraction of the Fermi wavelength: say $\Delta R \simeq \lambda_f/4$ or $\lambda_f/3$ (this is supported by the perturbation approach exposed in Appendix B). This estimate leads to a separation of the quantum behaviors starting at $N \sim 150$ or 550. However, we will see that the dominant classical periodic orbits of the two systems are very different, and simply on the basis of the trace formula we would not expect such similar quantum behavior if we were to believe semiclassical results down to the bottom of the spectrum.

IV. SEMICLASSICAL THEORY

Oscillations in the density of states such as those responsible for the shell structure have been very successfully predicted in terms of classical periodic orbits according to the theory of Gutzwiller (see, e.g., Ref. 22 and references therein) and Balian and Bloch.[23] In this theory, oscillations in the density of states are expressed directly as a sum over periodic orbits of the corresponding classical system.

In this section, we attempt to interpret the shell oscillations of Fig. 1 within this framework. The formalism works very well for the oscillations of longest scale in $N^{1/3}$, corresponding to the shortest periodic orbit, but fails for shorter scales. We interpret this failure as being due to diffractive effects which are not included in a direct use of the periodic orbit formula.

The original formulation of Gutzwiller applies to cases where classical periodic orbits of a given energy are isolated in phase space, such as occurs in (classically) chaotic systems. This is not the case for the icosahedral billiard, however, because orbits occur in two-parameter families due to a symmetry that corresponds to a local translation of orbits parallel to the faces of the icosahedron. If a given periodic orbit has an even number of bounces, it is possible to deform it into another nearby periodic orbit by translating it at any point where it bounces from a face along any of the two dimensions parallel to that face. A similar degeneracy of orbits occurs in the case of the spherical cavity due to the three-parameter rotational symmetry of that system. As one would expect, the higher the degree of degeneracy of periodic orbits, the larger the resulting oscillations in the density of states. Thus the oscillations in the icosahedron are larger than in a typical chaotic system, but smaller than in the spherical cavity.

We use a generalization of the Gutzwiller theory that is valid for the case of degenerate periodic orbits.[24] Here we quote the result as it applies to the icosahedron and leave detailed discussion for the future.[16] The main contribution to the oscillating level density can be written as (see Ref. 16)

$$\tilde{\rho}(k) \simeq \frac{k\nu}{2\pi^2} \sum_{\text{PPO}} \sum_{r=1}^{+\infty} \frac{\mathcal{S}}{r} \mathcal{A} \cos\phi \sin(krL) \ . \tag{21}$$

In formula (21) L is the length of a primitive periodic orbit (PPO), and r labels the repetitions of this orbit. $\mathcal{A}$ is

the area occupied by the orbit on a face and ϕ the angle between the direction of the orbit and the normal to this face. $\mathcal{S}$ is a symmetry factor counting the number of distinct orbits obtained by applying one of the elements of the icosahedron's symmetry group to the primitive periodic orbit; for instance, for the pendulating orbit below $\mathcal{S}=10$ (the orbit links 2 by 2 the 20 faces of the icosahedron).

Since we are only interested in shell effects, i.e., in the gross features of the level density, we need only determine the shortest PO's of the system. There are two significant orbits in the icosahedron, with approximate lengths $3.0a$ and $5.6a$, respectively—all other orbits were found to have much longer length and/or smaller cross-sectional area $\mathcal{A}$. The interesting orbits are the pendulating and the bow-tie orbits shown in Fig. 2. They each form a two-parameter family and they occupy the area shaded in Fig. 2. Their characteristics are listed in Table II. As mentioned before, the main classical PO's in the sphere have very different properties: the pendulating orbit indeed exists (as a two-parameter family) but it plays a negligible role in comparison with the other orbits, which form three-parameter families (the shortest being the triangle and the square, see Ref. 23). Thus we already see that leading oscillating contributions (21) cannot account for the similarities of the quantum behavior of the icosahedron and the sphere that are observed at low values of N.

Since typical orbits have a length of order $L\sim a\sim N^{1/3}$, from Eq. (21) one sees that the level density at the Fermi energy (and all other related quantities) oscillates with a period of order $N^{1/3}$ as the size of the cluster increases (see Fig. 1). The qualitative features of the oscillations in physical quantities are discussed in Appendix C using a schematic form of $\tilde{\rho}(k)$.

One can obtain a more quantitative comparison between the computed level density and the semiclassical estimation (21) by convoluting the exact spectrum with a smoothing function $w(k)$. Then formula (12) reads

$$\rho_{\mathrm{conv}}(k)=\nu\sum_n d_n w(k-k_n)\ . \tag{22}$$

Without displaying all the explicit formulas (see Ref. 16), let us mention that the convolution of (21) yields a trace formula for $\tilde{\rho}_{\mathrm{conv}}$ where the periodic orbits of length L are damped by a weight factor $\hat{w}(L)$, where $\hat{w}(L)$ is the Fourier transform of $w(k)$. If $\hat{w}(L)$ decreases rapidly—i.e., if $w(k)$ is broad—long PO's will not contribute to $\tilde{\rho}_{\mathrm{conv}}$.

We choose $\hat{w}$ in order to be able to discriminate efficiently orbits with similar lengths. It was taken to be

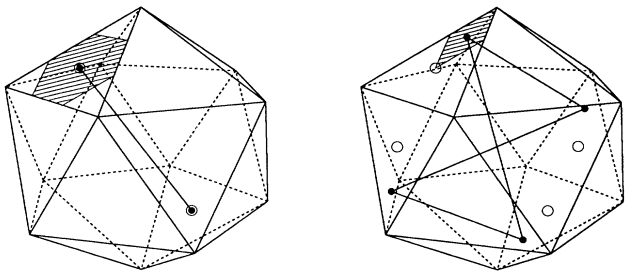

FIG. 2. The two shortest periodic orbits in the icosahedron. The shaded area indicates the surface occupied by the family. To make the trajectories more easy to visualize, we placed a white spot on the center of each face hit by the orbit. Each bouncing point on a face is marked with a black spot.

the convolution of a step function θ (A-L) with a Gaussian (standard deviation σ). Figure 3 shows the comparison of $\tilde{\rho}_{\mathrm{conv}}$ [computed from Eq. (21)] with $\rho_{\mathrm{conv}}-\bar{\rho}$ [computed from Eq. (22) using the numerically computed eigenvalues] when $A=2.3a$ and $\sigma=0.6a$. As seen in the figure this choice of parameters (A,σ) selects only the pendulating orbit, and the agreement between the quantum and semiclassical results is very satisfactory.

The agreement is not so good, however, if A is increased slightly so as to allow slightly longer orbit lengths to play a role. Figure 4 shows the same comparison for $A=3.5a$ and $\sigma=0.6a$. From Eq. (21) one would not expect any qualitative change with respect to Fig. 3 since the bow-tie orbit is still discarded by the weighting function $\hat{w}(L)$ (it has a length $\simeq 5.65a$). A Fourier analysis of the spectrum reveals oscillations corresponding to a classical length of $L\sim 4.0a$. We have searched intensively for periodic orbit families in this length range and found none. Therefore we are forced to conclude that there are classical structures responsible for spectral fluctuations which are not of the form of Eq. (21).

It is possible to think of two types of correction to the periodic orbit formula that might explain this anomalous behavior.

(i) Orbits with an odd number of bounces. Such orbits do not remain periodic when a point of reflection is translated along a face (they period double into periodic orbits with twice as many bounces) and form one-parameter families. They would therefore contribute to $\tilde{\rho}$ with a factor of order $k^{-1/2}$ less than the two-parameter families.

(ii) Orbits bouncing on an edge or a vertex. According to Keller's "geometrical theory of diffraction" (see, e.g.,

TABLE II. Parameters characterizing the two shortest orbits in the icosahedron [see Eq. (21)]. L is expressed in units of the edge length a. $\mathcal{A}$ is in units of a^2.

Orbit	L	$\mathcal{A}$	$\mathcal{S}$	$\cos\phi$
Pendulating	$\frac{3+\sqrt{5}}{\sqrt{3}}\simeq 3.023$	$\frac{\sqrt{3}}{6}\simeq 0.289$	10	1
bow-tie	$\frac{4}{3}(2+\sqrt{5})\simeq 5.648$	$\frac{\sqrt{3}}{18}\simeq 0.096$	30	$\frac{1+\sqrt{5}}{2\sqrt{3}}\simeq 0.934$

Ref. 25) such orbits can be used to explain diffractive effects—we will therefore refer to them as "diffractive orbits." Each diffraction from an edge decreases the contribution to the trace formula by order $k^{1/2}$, and from a vertex by order k. If these orbits occur in one-parameter families or are isolated, their contributions are further reduced by orders $k^{1/2}$ or k, respectively.

Notice that each of these possible contributions is of higher order in k, and should therefore be insignificant for large enough clusters. However, it is evident that this regime is not yet reached for the stretch of spectrum that we found numerically.

Of the two possibilities above, (i) can be eliminated as an explanation of the anomalous behavior in Fig. 4, because there is no orbit with an odd number of bounces that is short enough. Therefore (ii) seems to be the only possible explanation, and we are led to conclude that diffractive effects play an important role in determining the oscillating level density for moderate values of k in the icosahedron. We would expect the same conclusion to hold for any billiard with nontrivial sharp edges (by "nontrivial" we mean that edges with the same angle, etc. do not occur in simpler tessellating billiards). We will study this phenomenon in a forthcoming paper.[16]

The diffraction effects discussed here obviously cannot be relevant in a detailed way for physical clusters, since the sharp edges are an artificial feature of the model.

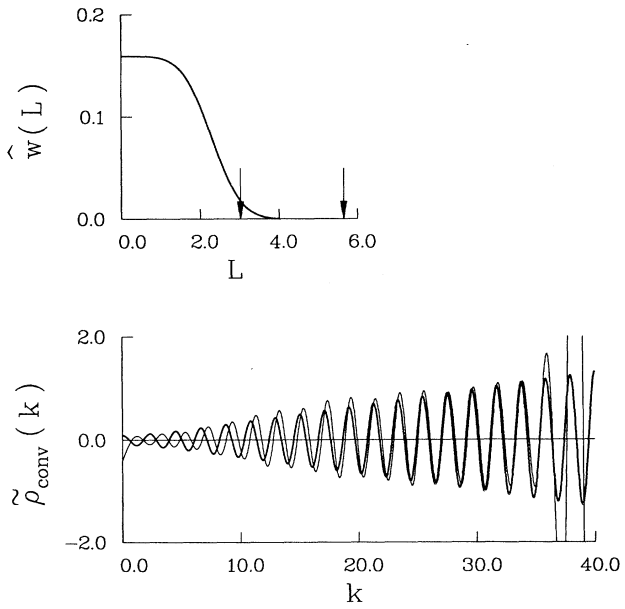

FIG. 3. $\tilde{\rho}_{conv}$ as a function of k (lower part) for a function $\hat{w}(L)$ (upper part) characterized by the coefficients $A=2.3$ and $\sigma=0.6$. The arrows indicate the length of the pendulating and of the bow-tie orbit. The lengths are in units of a, and the momenta in units of $1/a$. In the lower graph the thick line represents the semiclassical prediction, and the thin line is the quantum result. Due to the convolution the quantum results stop being relevant here at $k\simeq 32/a$: our computation extends up to $k\simeq 40/a$, and the exact convolution (22) becomes sensitive to this upper boundary.

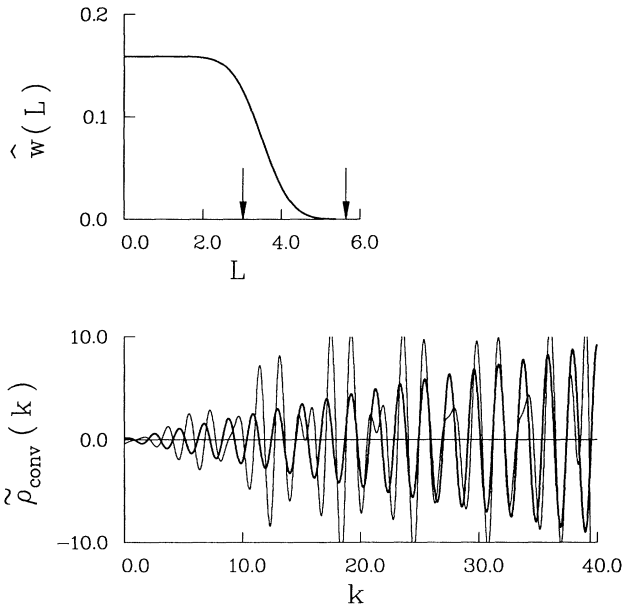

FIG. 4. Same as Fig. 3 for a function $\hat{w}(L)$ characterized by $A=3.5$ and $\sigma=0.6$. Since $w(k)$ is extended less here than in Fig. 3, the "boundary effects" near $ka=40$ for the quantum result are less important.

However, they do indicate a mechanism through which the real spectrum deviates from the simple semiclassical spectrum for small clusters. Such a deviation is also indicated by a surprising degree of agreement between spherical and icosahedral results at the low values of k examined, despite the disparity of the semiclassical pictures. In the limit of short wavelengths, however, these diffraction effects are presumably not important, even in our billiard model. We have not been able to determine enough of the spectrum to evaluate precisely where this transition to semiclassically predicted behavior occurs.

Therefore, as the cluster size increases, we expect that the shell oscillations will be given more nearly by formula (21), without diffractive effects. Thus we evaluate the large-N behavior of $\tilde{E}_{tot}$ using Eq. (21) with the four shortest families of periodic orbits of the system. This leads to the pattern displayed in Fig. 5. As explained in Appendix C, the amplitude of the oscillations is approximately constant for large N. The interference between the bow-tie orbit ($L=5.6a$) and the repetition of the pendulating orbit ($2L=6.0a$) are responsible for the modulation of $\tilde{E}_{tot}$. These two orbits contribute to the PO sum (21) with different prefactors, and the interference is also obscured by the presence of the simple pendulating orbit. As a result there is here no strong beating pattern such as caused in the sphere by the contributions of the triangle and square.[23]

Comparing Figs. 1 and 5 one sees that at $N^{1/3}=16$ the "true semiclassical limit" where Eq. (21) holds without diffraction corrections is not yet reached. However, the amplitude of the oscillations at $N^{1/3}\simeq 16$ in Fig. 1 is about what is expected semiclassically. Hence, for larger N we expect the amplitude of the exact shell effect to

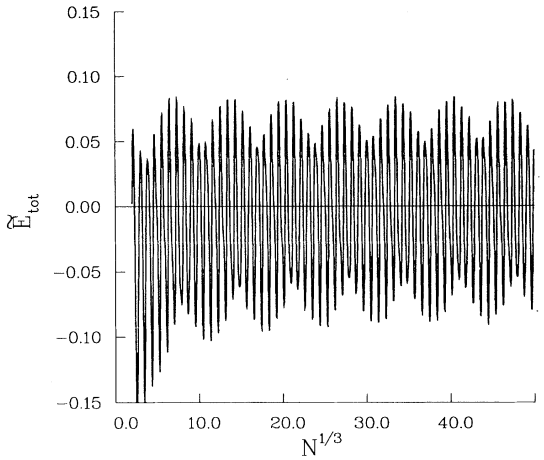

FIG. 5. Semiclassical estimation of $\tilde{E}_{tot}$ including the four shortest PO's in summation (21) (as explained in the text, here we consider only orbits with even number of bounces). $\tilde{E}_{tot}$ is expressed in units of ε_f (the bulk Fermi energy).

remain approximately constant and equal to the semiclassical prediction. For still larger values of N the exact magic numbers should match the predictions of Fig. 5.

V. DISCUSSION

In this paper we have studied the electronic shell structure in an icosahedral cluster, using the simple model of an infinite potential well. We have found that the magic numbers for this system are the same as those for a spherical well up to $N \sim 350$, and this can be understood to arise because of the similarity in shape between the sphere and the icosahedron.

Our results reveal a useful criterion for distinguishing between spherical and faceted structures: the existence of quantum shells up to $N \sim 1400$ electrons in the experiment of Ref. 3 is not a very conclusive sign of the sphericity of the clusters studied. This can be seen by comparing the theoretical magic numbers in spherical and faceted clusters with their measured values (Table I): it is often difficult to decide which of the two models is in better agreement with the experiments. A more conclusive approach is to study the supershell structure using the procedure exposed in Ref. 8: the supershells can be revealed from a plot of the cube root of the magic numbers $(N_{mag})^{1/3}$ against a running index i labeling the shells. In the case of interference of the two main orbits (as is the case for a spherical cluster), there is a phase shift $\delta i = \frac{1}{2}$ in the nodal region of the beating pattern. No such phase shift can be detected for the icosahedron in the region where the experiments find it [$N \simeq 800$ (Refs. 2, 5, and 8)], whereas the spherical model predicts its location quite accurately.

Regarding the distinction between electronic and atomic shell structures, one of the more important results is the following observation of Ref. 3: above $N \sim 1500$ electrons the index labeling the magic numbers still grows like $(N_{mag})^{1/3}$, but with a completely different slope from that predicted by the electronic shell structure. This change in behavior has been explained by the transition to completion of icosahedral shells of atoms rather than the filling of electronic shells as being the dominant factor in cluster formation. Our computations extend up to $N \simeq 4200$ electrons, and no such changes in the magic structure can be detected (see Fig. 1). This indicates that when clusters become "solid" the electrons play a minor role in determining stable configurations, and that most of the total binding energy is due to the atomic structure. However, the results of Ref. 3 are peculiar in the sense that, contrary to what is seen at higher temperature,[5,8] no magic phase shift is seen in the "quantum region" at $N \simeq 800$. We interpret this absence of the supershell as a signature of the nonsphericity of the clusters studied in Ref. 3. It could be due to strong deformations (maybe with icosahedral symmetries) of still liquid clusters.

We have made an attempt at interpreting the electronic shell structure in the icosahedron in terms of PO's. The semiclassical approach used in spherical cavities[23] does not extend so successfully here. However, we argue that semiclassical arguments are still useful to evaluate the amplitude of the shell oscillations in large clusters, and that they would predict accurately the magic numbers of the model in the large N limit.

Finally, let us mention that the billiard model we use here has its own interest within the general framework of semiclassical approximations. Our study suggests that the diffractive orbits represent an important contribution to the trace formula at low energy. We will address this question in a future work.

ACKNOWLEDGMENTS

We thank E. Bogomolny and C. Schmit for their interest in this study and for the advice they provided us at all the stages of this work. We also thank A. Bulgac for comments on the manuscript. We are particularly indebted to A. Le Guillou and the Malakoff group for fruitful exchanges and discussions. S.C. was supported under the programme of the Commission of the European Communities under Contract No. S/SC1*/915161. Division de Physique Théorique is Unité de Recherche des Universités Paris XI et Paris VI associée au CNRS.

APPENDIX A

In this appendix we discuss the effects of random fluctuations in the ionic background on the model calculated in the main text.

In any real cluster, the ionic background will have significant random fluctuations which will alter significantly the effective background potential experienced by the electrons. For the purposes of our system, one might model these effects as fluctuations in the interior potential and in the shape of the boundary, corresponding to the placement of individual ions. For example, if there are not enough atoms to completely fill an atomic shell, one might imagine lumps in the potential at the surface, corresponding to the random positions of ions within an incomplete outer shell.

We argue here that even if these fluctuations are enough to make a smooth featureless potential such as the one we use invalid for an *individual* cluster, it is necessary in practice to average over an experimental ensemble, and the effect of this is to validate a model in which the bumps caused by the ions are averaged out.

In an experiment where many clusters of each size are detected, the relevant quantity determining the probability of formation of clusters is the following averaged density of states:

$$\rho_{\rm av}(k)=\langle\rho_\alpha(k)\rangle_\alpha=\sum_n\langle\delta(k-k_n^{(\alpha)})\rangle_\alpha\ , \tag{A1}$$

where the average is taken over cluster configurations α within some ensemble. The levels and density of states of configuration α are denoted by $k_n^{(\alpha)}$ and $\rho_\alpha(k)$, respectively.

Let us model the experimental ensemble by the set of Hamiltonians

$$H_\alpha=H_0+V_\alpha\ , \tag{A2}$$

where H_0 is a simple Hamiltonian such as the one used by us, and V_α represents some random background fluctuation corresponding to a given ionic configuration. Each eigenlevel k_n of H_0 is perturbed to $k_n+\Delta k_n^{(\alpha)}$ when V_α is included—let $w_n(\Delta k)$ represent the distribution function for the shifts $\Delta k_n^{(\alpha)}$ within the ensemble. Then the averaged density of states is

$$\rho_{\rm av}(k)=\sum_n w_n(k-k_n)\ . \tag{A3}$$

We now make the assumption that $w_n(\Delta k)$ depends on n only through some weak dependence on k_n. This certainly seems reasonable if the size of V_α is such that the shifts are of the order of many level spacings—then each shift will be affected by a statistically large group of levels within some energy range, and all levels within that range should be affected in more or less the same way by the ensemble of perturbations. However, this is only an assumption. Such a weak k_n dependence will not alter qualitatively the following discussion, so we will denote the distribution of shifts simply by $w(\Delta k)$. Then,

$$\rho_{\rm av}(k)=w_*\rho_0(k)\ , \tag{A4}$$

where $w_*\rho_0$ represents the convolution of the function w with the density of states ρ_0 of H_0.

Therefore, the effect of random fluctuations is just to smooth out the density of states of H_0 with some distribution function. Such a procedure does not alter qualitatively the shell oscillations calculated in this paper. In terms of the discussion of Sec. IV, the effect is to damp the contribution to the density of states of longer orbits relative to that of shorter orbits—the contributions of orbits of length L are modified by a factor $\hat{w}(L)$, the Fourier transform of $w(k)$.

Note that these arguments work more convincingly in justifying the use of a spherical cavity for small clusters than they do in justifying the icosahedral cavity for larger clusters. In the spherical case, the clusters are "liquid" and the averaged potential would truly be spherical, and flat in the interior. In the icosahedron, correlations of the ions would remain with their preferred positions with respect to the lattice, and the true averaged potential would be lumpy. However, the argument still works to show that this lumpiness is less than one would expect from considering an individual cluster. In addition, it suggests that this model should work best for high-temperature clusters.

APPENDIX B

In this appendix we estimate typical energies linked to the deformation of an initially spherical potential. We use a simple perturbation theory valid for a system with infinite walls.[26] The shape of the deformed particle will be expressed in direction $\hat{\mathbf{e}}$ by a development on spherical harmonics:

$$r_B(\hat{\mathbf{e}})=R\left[1+\sum_{\lambda=1}^{+\infty}\sum_{\mu=-\lambda}^{+\lambda}b_{\lambda\mu}Y_{\lambda\mu}(\hat{\mathbf{e}})\right]\ . \tag{B1}$$

In the following all the $b_{\lambda\mu}$'s will be considered as small parameters. Accordingly, at zeroth order the volume enclosed in boundary (B1) is a sphere of radius R. We will consider here two types of surface deformations and compare the changes in energy they induce.

(1) Small bumps of order r_s on the surface. In this case $\lambda-\mu$ and μ are of order $N^{1/3}$ and $b_{\lambda\mu}\sim r_s/R\sim N^{-1/3}$.

(2) For an icosahedral cluster the linear combination of $Y_{\lambda\mu}$'s in (B1) must belong to the trivial irrep of I_h (this selects $\lambda=6,10,12,16,\ldots$). The $b_{\lambda\mu}$'s are at most of order $(R-a)/R\sim 0.1$, and decrease for increasing angular momentum.

Without taking into account the possible symmetries of the surface specified by (B1), the matrix elements $M_{ij}(k)$ here read [compare with Eq. (7)]

$$M_{ij}(k)=\int d\Omega\, j_l(kr_B(\hat{\mathbf{e}}))Y^*_{l'm'}(\hat{\mathbf{e}})Y_{lm}(\hat{\mathbf{e}})\ , \tag{B2}$$

where $i(j)$ is here an index labeling the pair of quantum numbers (l,m) $[(l',m')]$.

Then we make a limited expansion of $j_l(kr_B(\hat{\mathbf{e}}))$ around kR, yielding

$$M_{ij}(k)\simeq j_l(kR)\delta_{ij}+kRj_l'(kR)\sum_{\lambda\mu}b_{\lambda\mu}\int d\Omega\, Y_{\lambda\mu}Y^*_{l'm'}Y_{lm}\ , \tag{B3}$$

where δ_{ij} is a short notation for $\delta_{ll'}\delta_{mm'}$. From (B3) the matrix $M(k)$ is expressed as a sum of a diagonal matrix [let us call it $J(k)$] plus a matrix $A(k)$:

$$M(k)=J(k)+A(k)\equiv J(k)+kJ'(k)B\ . \tag{B4}$$

In the second line of Eq. (B4) we have made explicit the k dependence of matrix $A(k)$. $J'(k)$ is the derivative of $J(k)$; B is a k-independent matrix defined by comparing (B3) and (B4); its coefficients are of the order of the $b_{\lambda\mu}$'s. Then it is natural to write

$$\det M = \exp(\mathrm{Tr}\ln(M)) = \det J + \det J\ \mathrm{Tr}(J^{-1}A) + \dots . \quad \text{(B5)}$$

From (B5) one can evaluate the zeros of $\det\{M(k)\}$ easily. We write them as

$$k_{nlm} = k^0_{nl} + \Delta k_{nlm} , \quad \text{(B6)}$$

where the k^0_{nl}'s are the zeros of $\det\{J(k)\}$. They are the unperturbed levels, solutions of $j_l(k^0_{nl}R)=0$. From (B4) and (B5), a limited expansion yields after simple manipulations

$$\Delta k_{nlm} = -\frac{\mathrm{Tr}\{J^{-1}(k^0_{nl})A(k^0_{nl})\}}{\mathrm{Tr}\{J^{-1}(k^0_{nl})J'(k^0_{nl})\}} . \quad \text{(B7)}$$

From the explicit k dependence of matrix A (B4) we deduce that the relative shift of the eigenlevel $\Delta k_{nlm}/k^0_{nl}$ is of the order of the matrix elements of B, i.e., of the order of the $b_{\lambda\mu}$'s. We see—as stated in Sec. I—that faceting will affect the eigenenergies with a factor $N^{1/3}$ larger than surface bumps.

Of course there is an important drawback to the perturbation method presented here: it is strictly valid only for wave vectors such that $kR\langle b_{\lambda\mu}\rangle \ll 1$, i.e., for wavelengths large compared to the surface deformation. This is the reason why trying to get a quantitative estimate of the shell structure in a faceted cluster using perturbation theory is a difficult task. However, this does not affect the qualitative picture presented here: the surface defects involve a part of the total volume of the cluster which is smaller by a factor $N^{-1/3}$ than the facets, and the characteristic energies are accordingly smaller.

APPENDIX C

In this appendix we estimate the amplitude of the shell oscillations (for $\tilde{E}_f$ and $\tilde{E}_{\mathrm{tot}}$) in large clusters (i.e., large N). Because we are only interested in rough estimates of the relative sizes of the oscillatory and the averaged contributions, we include only the contribution of a single periodic orbit to the oscillatory part, and use only the leading term in the expansion Eq. (14) for the averaged part of the density of states as follows:

$$\tilde{\rho}(k) \simeq Ca^2 k \sin(kL) , \quad \bar{\rho}(k) \simeq 3a_v a^3 k^2 . \quad \text{(C1)}$$

Here a and L are of order $r_s N^{1/3}$. C is a dimensionless constant, uninteresting for the purposes of this appendix.

The relation defining k_f reads

$$N = \int_0^{k_f} [\bar{\rho}(k)+\tilde{\rho}(k)]dk \simeq a_v a^3 k_f^3 - C\frac{a^2 k_f}{L}\cos(k_f L) . \quad \text{(C2)}$$

Here we neglect an oscillating term $C(a/L)^2\sin(k_f L)$, which is smaller than the oscillating term of (C2) by a factor of order L. For large N, the smooth term dominates in (C2) and we can invert this part to express k_f as a smooth function of N, on top of which small oscillatory corrections are to be added:

$$k_f \simeq \frac{(N/a_v)^{1/3}}{a}[1+\epsilon(N)] . \quad \text{(C3)}$$

The leasing term is denoted by $\bar{k}_f$ and is of order 1 (more precisely $1/r_s$) for larger N. A limited expansion for the remaining oscillatory contribution yields

$$\epsilon(N) \sim \frac{C}{3a_v^{1/3}}\frac{a}{L}(N)^{-2/3}\cos\left[\frac{L}{a}(N/a_v)^{1/3}\right] . \quad \text{(C4)}$$

As noted in the text, the oscillations are equally spaced in $N^{1/3}$. From (C3) and (C4) we see that the amplitude of the oscillations in $\tilde{k}_f$ behave for large N as

$$\tilde{k}_f \sim \bar{k}_f N^{-2/3} , \quad \text{(C5)}$$

and $\tilde{E}_f$ scales similarly with N.

The oscillations in the total energy are computed from the differences between the quantities E_{tot} and $\bar{E}_{\mathrm{tot}}$:

$$E_{\mathrm{tot}} = \int_0^{k_f}\frac{\hbar^2k^2}{2m}[\bar{\rho}(k)+\tilde{\rho}(k)]dk , \qquad \bar{E}_{\mathrm{tot}} = \int_0^{\bar{k}_f}\frac{\hbar^2k^2}{2m}\bar{\rho}(k)dk . \quad \text{(C6)}$$

Then,

$$\begin{aligned}\tilde{E}_{\mathrm{tot}} &= E_{\mathrm{tot}} - \bar{E}_{\mathrm{tot}} \\ &= \int_{\bar{k}_f}^{k_f}\frac{\hbar^2k^2}{2m}\bar{\rho}(k)dk + \int_0^{k_f}\frac{\hbar^2k^2}{2m}\tilde{\rho}(k)dk \\ &\simeq (k_f-\bar{k}_f)\frac{\hbar^2\bar{k}_f^2}{2m}\bar{\rho}(\bar{k}_f) + \int_0^{\bar{k}_f}\frac{\hbar^2k^2}{2m}\tilde{\rho}(k)dk . \end{aligned} \quad \text{(C7)}$$

In (C7) we replaced the integrals by their large-N approximations. The two terms on the right-hand side of Eq. (C7) cancel exactly at leading order (i.e., at order $N^{1/3}$). Thus in (C7) the dominant term is constant for large N:

$$\tilde{E}_{\mathrm{tot}} \sim \varepsilon_f , \quad \text{(C8)}$$

where ε_f is the asymptotic value of the Fermi energy. The detailed structure of the semiclassical estimate of $\tilde{E}_{\mathrm{tot}}$ is displayed in Fig. 5.

We recall that in the case of a sphere of radius R the main orbits form three-parameter families, and the oscillating level density reads schematically

$$\tilde{\rho}_{\mathrm{sph}}(k) \simeq R(Rk)^{3/2}\sin(kL) . \quad \text{(C9)}$$

This leads to large-N behaviors for $\tilde{E}_f$ and $\tilde{E}_{\mathrm{tot}}$ that are different from those of the icosahedron. Repeating the procedure above for the sphere, one obtains

$$\tilde{E}_f \sim \varepsilon_f N^{-1/2} \quad \text{and} \quad \tilde{E}_{\mathrm{tot}} \sim \varepsilon_f N^{1/6} . \quad \text{(C10)}$$

[1]S. Bjørnholm, J. Borggreen, O. Echt, K. Hansen, J. Pedersen, and H. D. Rasmussen, Phys. Rev. Lett. **65**, 1627 (1990).
[2]C. Bréchignac, Ph. Cahuzac, F. Carlier, M. de Frutos, and J. Ph. Roux, Phys. Rev. B **47**, 2271 (1993).
[3]T. P. Martin, T. Bergmann, H. Göhlich, and T. Lange, Z. Phys. D **19**, 25 (1991).
[4]T. P. Martin, T. Bergmann, H. Göhlich, and T. Lange, Chem. Phys. Lett. **176**, 343 (1991); T. P. Martin, U. Näher, T. Bergmann, H. Göhlich, and T. Lange, *ibid.* **183**, 119 (1991).
[5]T. P. Martin, S. Bjørnholm, J. Borggreen, C. Bréchignac, Ph. Cahuzac, K. Hansen, and J. Pedersen, Chem. Phys. Lett. **186**, 53 (1991).
[6]H. Nishioka, K. Hansen, and B. R. Mottelson, Phys. Rev. B **42**, 9377 (1990).
[7]P. Stampfli and K. H. Bennemann, Phys. Rev. Lett. **69**, 3471 (1992); P. Stampfli and K. H. Bennemann, Z. Phys. D **25**, 87 (1992).
[8]J. Pedersen, S. Bjørnholm, J. Borggreen, K. Hansen, T. P. Martin, and H. D. Rasmussen, Nature **353**, 733 (1991).
[9]J. Lermé, M. Pellarin, J. L. Vialle, B. Baguenard, and M. Broyer, Phys. Rev. Lett. **68**, 2818 (1992).
[10]A. Maiti and L. M. Falicov, Phys. Rev. A **44**, 4442 (1991).
[11]J. Mansikka-aho, E. Hammarén, and M. Manninen, Phys. Rev. B **46**, 12 649 (1992).
[12]O. Genzken and M. Brack, Phys. Rev. Lett. **67**, 3286 (1991).
[13]K. Clemenger, Phys. Rev. B **44**, 12 991 (1991).
[14]S. Iijima and T. Ichihashi, Phys. Rev. Lett. **86**, 616 (1986).
[15]E. L. Nagaev, Phys. Rep. **222**, 200 (1992).
[16]S. C. Creagh and N. Pavloff (unpublished).
[17]C. Schmit, in *Chaos and Quantum Mechanics,* edited by M. J. Giannoni, A. Voros, and J. Zinn-Justin, Les Houches Summer School Lectures LII, 1989 (North-Holland, Amsterdam, 1991).
[18]Wu-Ki Tung, *Group Theory in Physics* (World Scientific, Philadelphia, 1985).
[19]W. H. Press, B. P. Flannery, S. A. Teukolsky, and W. T. Vetterling, *Numerical Recipes* (Cambridge University Press, Cambridge, 1986).
[20]H. Baltes and E. R. Hilf, *Spectra of Finite Systems* (Bibliographisches Institut, Mannheim, 1976).
[21]A. Bohr and B. R. Mottelson, *Nuclear Structure II* (Benjamin, New York, 1975), p. 578.
[22]M. C. Gutzwiller, *Chaos in Classical and Quantum Mechanics* (Springer-Verlag, New York, 1990).
[23]R. Balian and C. Bloch, Ann. Phys. (N.Y.) **69**, 76 (1972).
[24]S. C. Creagh and R. G. Littlejohn, Phys. Rev. A **44**, 836 (1991).
[25]G. L. James, *Geometrical Theory of Diffraction for Electromagnetic Waves* (Peregrinus, Stevenage, 1976).
[26]C. Schmit (private communication).